AIP | Applied Physics Letters

Production of carbonaceous nanostructures from a silver-carbon ambient spark

Jeong Hoon Byeon and Jang-Woo Kim

Citation: Appl. Phys. Lett. **96**, 153102 (2010); doi: 10.1063/1.3396188
View online: http://dx.doi.org/10.1063/1.3396188
View Table of Contents: http://apl.aip.org/resource/1/APPLAB/v96/i15
Published by the American Institute of Physics.

Production of carbonaceous nanostructures from a silver-carbon ambient spark

Jeong Hoon Byeon[1] and Jang-Woo Kim[2,a)]
[1]*LCD Division, Samsung Electronics Co., Ltd., Yongin 446-711, Republic of Korea*
[2]*Department of Digital Display Engineering, Hoseo University, Asan 336-795, Republic of Korea*

(Received 17 February 2010; accepted 25 March 2010; published online 14 April 2010)

Using silver-carbon ambient sparks, hollow carbon nanospheres or multiwall carbon nanotubes were produced separately from carbon encapsulated silver nanoparticles ($-1,400$ K s^{-1}) during relatively slow (-800 K s^{-1}) or fast ($-2,900$ K s^{-1}) cooling process. Different cooling processes (i.e., different exposures within high temperature) caused the formation of different carbon precipitates in the process of silver mediated graphitization: for $-2,900$ K s^{-1} and $<-1,400$ K s^{-1}, respectively, obtained tubelike and sphere (encapsulated and hollow)-like carbonaceous nanostructures. © *2010 American Institute of Physics*. [doi:10.1063/1.3396188]

Nowadays, some carbonaceous structures related with fullerenes and carbon nanotubes are recognized as interesting nanomaterials, e.g., hollow spheres, onions, horns, and coils.[1] Among these materials, metal-included nanostructures were especially interesting as they are promising materials for electromagnetic applications and micromachine technologies.[2] Moreover, the unique electrical and mechanical properties of the nanostructures make them promising candidates for field-effect transistors, nanoscale coaxial cables, electromechanical actuators, and other nanoelectronic elements and systems.[3]

Silver nanoparticles have attracted a great deal of interest in recent years because these materials are good candidates that can be applied for optics,[4] electronics,[5] and catalysis.[6] The modification of nanoparticles is found to be a powerful tool for drastically changing and precisely tuning their optical, mechanical, and surface properties.[7] Recently, much work has been done on the fabrication of silver hybrid materials, such as silver-carbon core-shell[7–11] and silver coated carbon nanoparticles.[12,13]

Ambient spark discharge[14] of a silver-carbon configuration was selected in the present work for an aerosol fabrication of carbonaceous nanostructures as a convenient platform. The spark discharge is a kind of atmospheric-pressure nonequilibrium discharges.[15] While the collision rate of electrons, ions, and neutrals is high, the discharge does not reach thermal equilibrium because it is short-lived, being interrupted before an arc discharge[16] is formed through. Carbonaceous nanostructures have been generally fabricated by vapor deposition, e-beam irradiation, and arc discharge techniques with the assistance of high vacuum and power (>1 kW). Recently, carbon encapsulated nanoparticles with transition metals were fabricated using spark discharge as the aerosol synthesis system under ambient conditions.[17,18] On the other hand, a controllable fabrication of carbonaceous nanostructures will be significant for their selective fabrication and provide insights into their formation mechanism.[19] Therefore, in the present work, the we reported the creation of different carbonaceous nanostructures such as carbon encapsulated silver nanoparticles, carbon nanotubes, and hollow carbon nanospheres by controlling the flow rate of the operation gas into the spark. The silver was used as a unique model to demonstrate the possibility of fabricating nanostructures because few works have reported their fabrication from a silver-carbon configuration.

A spark [Fig. 1(a)] was generated between the silver and graphite carbon rods (diameter: 3 mm, length: 100 mm, Nilaco, Japan) inside a reactor within a pure nitrogen (10^{-4} impurities) environment at standard temperature and pressure. The electrical circuit specifications were as follows: a resistance of 0.5 MΩ; a capacitance of 10 nF; a loading current of 2.2 mA; an applied voltage of 2.8 kV; and a frequency of 600 Hz (i.e., spark duration of 1.67 ms). The flow rate of the nitrogen gas was controlled by a mass flow controller (MFC). The cooling rate (R_c) is defined as follows:

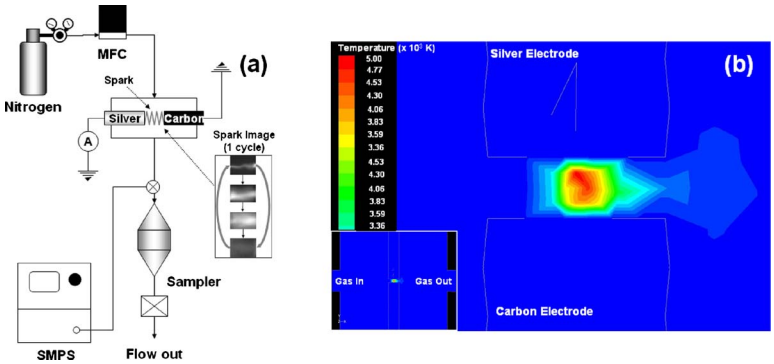

FIG. 1. (Color online) (a) Schematic of spark discharge system and high speed camera images of spark. (b) Temperature contour near spark channel for $\sim -1,400$ K s^{-1}.

a)Author to whom correspondence should be addressed. Electronic mail: jwkim@hoseo.edu.

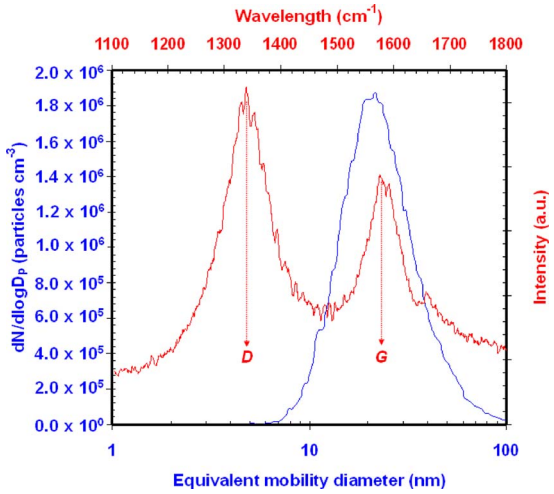

FIG. 2. (Color online) Particle size distribution and Raman spectrum for $\sim -1,400$ K s^{-1}.

$$R_c = V_g G_T, \tag{1}$$

where, V_g is the gas velocity and G_T is the temperature gradient between the spark channel and the surrounding ambient atmosphere. The temperature profile near the spark channel was simulated by the commercial computational fluid dynamics package (Fluent 6.0) with a spark channel temperature ($T_{spark} \sim 5,300$ K) estimated by the following formula:[20]

$$T_{spark} \sim \left(\frac{E_d}{C_v v_{spark} \rho_g} \right) + T_0, \tag{2}$$

where, E_d is the discharge energy, C_v is the specific heat at constant volume, v_{spark} is the volume of the spark channel, ρ_g is the gas density, and T_0 is the gas temperature. Figure 1(b) shows the computed temperature contour near the spark channel. The temperature of the nitrogen gas was high in the gap area between the electrodes, and it became lower when the gas passed through the gap to the surrounding atmosphere.

Figure 2 shows the size distribution of the spark produced aerosol nanoparticles measured using the scanning mobility particle sizer (SMPS) (TSI 3936; 4.61–163 nm detection range). The concentration, geometric mean diameter, and geometric standard deviation of the nanoparticles were 8.4×10^5 particles cm^{-3}, 22.3 nm, and 1.57, respectively. The data for $\sim -2,900$ (~ -800) K s^{-1} were 1.6×10^6 (7.3×10^4) particles cm^{-3}, 14.8 (84.3) nm, and 1.36 (1.62), respectively. The different cooling rates were probably represented by different coagulation coefficients with different gas flow rates (i.e., gas residence time, t), in accordance with the following equations:

$$\frac{N_0}{N} - 1 = \frac{K_0 N_0 t}{2} = \frac{t}{\tau}, \tag{3}$$

$$D_p = D_{p0} \sqrt[3]{N_0/N}, \tag{4}$$

where, N_0 and N are the initial and final particle number concentrations, respectively, K_0 ($K_0 = 8kT_0/3\mu$, where, k is the Boltzmann constant, and μ is the gas viscosity) is the collision frequency function, τ is the characteristic coagulation time, t/τ is the dimensionless coagulation time, and D_p and D_{p0} are the initial and final particle diameters, respectively. Although all the cases were operated at same electrical specifications for the sparks, the concentrations and sizes of the measured aerosol nanoparticles varied according to the cooling rate. A typical Raman (T64000, HORIBA Jobin Yvon) spectrum of the spark produced nanoparticles (also in Fig. 2) shows two main peaks centered at 1,338 (D band) and 1,575 cm^{-1} (G band). The G peak was due to bond stretching of all pairs of sp^2 carbon atoms in both the rings and chains, while the D peak was due to the breathing modes of the rings. The intensity ratio (I_G/I_D) between G and D bands was about 0.71, indicating the presence of a larger amount of sp^3 carbon than sp^2 carbon. The ratios for $\sim -2,900$ and ~ -800 K s^{-1} were 1.10 and 0.58, respectively, probably indicating a different formation of carbon precipitates in the silver mediated structuralization.

The transmission electron microscope (TEM) (JEM-3010, JEOL) images in Fig. 3(a) revealed the core to be darker (representing a higher density) than that of the shell, which also means that the particle had a metallic core with a carbon shell. Two to six graphene layers were observed around the dark core, and the size range of the particles was 15 ± 6 nm. The high resolution image [inset of Fig. 3(a)] of a particle core displays the lattice fringes with a spacing of 0.234 nm, which agreed well with that of cubic Ag (111). Silver formed no stable carbides and the solubility of carbon in silver is only 0.022 wt % (0.20 at. %) even at 1,660 °C.[21] The electron diffraction (ED) pattern [also in Fig. 3(a)] was a superposition of two patterns: a set of annular rings originating from graphene (diffraction from a two-dimensional lattice, $d_{002} = 0.341$ nm), and the other spots corresponding to the face centered cubic structure of silver ($a = 0.409$ nm, $d_{111} = 0.236$ nm). The diffraction pattern shows a diffused ring pattern with reflections of 0.35 and 0.21 nm^{-1}. These reflections corresponded to crystallographic planes (002) and (100, 101) of the graphite structure, which indicated that this phase had a turbostratic graphite structure. The feature discussed here concerned the graphitization of the carbon that led to the formation of graphene layers that were parallel to the surface of the silver nanoparticles. It is known that the interaction between carbon and a nonreactive metal could lead to a graphitization of carbon in order to reduce the system energy at low temperatures due to the presence of silver which served as catalyst. In order to verify the elemental composition of the nanoparticles, a measurement was performed using the energy dispersive x-ray (EDX) (JED-2300, JEOL) spectrometer attached to the scanning electron microscope (SEM) (JSM-6500F, JEOL) [Fig. 3(b)]. It could be

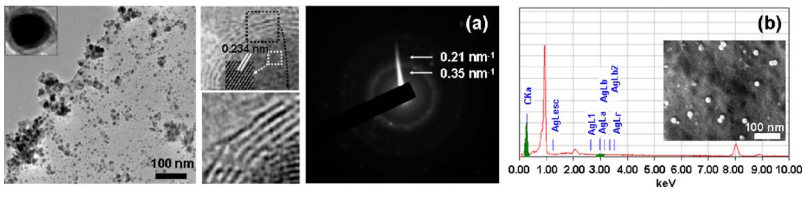

FIG. 3. (Color online) Results for carbon encapsulated silver nanoparticles. (a) TEM images and ED pattern. (b) EDX spectrum with SEM image.

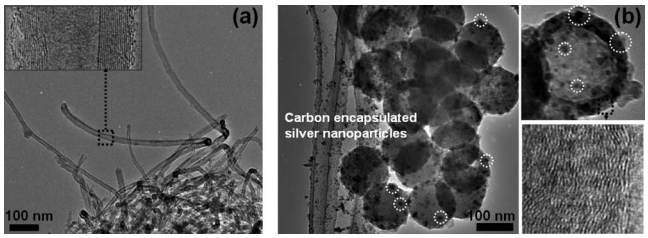

FIG. 4. TEM results for other nanostructures of (a) multiwall carbon nanotubes ($\sim -2{,}900$ K s^{-1}) and (b) hollow carbon nanospheres (~ -800 K s^{-1}).

suggested that the white spot spherical particles contained a silver element, which corresponded to silver peaks of AgLa1 and AgLb1 located at about 3.0 keV. The CKa signal was also detected for the particles, which was in accordance with a carbon encapsulated silver structure.

Figure 4(a) shows TEM images of multiwall carbon nanotubes with a ~16 (7) nm thick outer (inner) diameter which were fabricated at the cooling rate of $\sim 2{,}900$ K s^{-1}. The one dimensional carbon nanostructures between the surface-bound silver nanoparticles grew mainly by surface diffusion which delivered the carbon atoms to nanoparticles acting as growth catalysts.[3,22] Gadd *et al.*[23] (2001) mentioned that a relatively fast condensation (i.e., a relatively high cooling rate) favored incomplete encapsulation whereas fast condensation promoted the formation of nanotubes which grew from the solidifying metal particle. The influence of the gas flow rate on surface diffusion could affect a change in the surface diffusion activation energy, which in turn directly influenced the thermal flux on a part of surface and eventually introduced the growth of the nanotubes from silver nanoparticles (~15 nm in diameter of agglomerates). The influx rates of carbon atoms might also influence the growth of the nanotubes.[15] The mean length of the nanotubes was only ~800 nm, because to achieve otherwise, the carbon atoms must be supplied to the silver nanoparticles at a temperature that was high enough to obtain the growth of longer nanotubes.[1] Figure 4(b) is the TEM image of hollow carbon nanospheres (~ -800 K s^{-1}), showing the conservation of the spherical geometry and an outer diameter of ~140 nm. All nanospheres had a hollow cavity and the carbon shell was fairly uniform. The interlayer distance [also in Fig. 4(b)] between the graphene planes was ~0.354 nm, larger than that of normal graphite (~0.335 nm). This was an indication that the crystallinity of the carbon in the hollow spheres had yet to match that in graphite. Like in cobalt and copper, the solubility of the carbon in silver was very weak.[24] Therefore, a displacement of silver could occur during or just after condensation, and the silver atoms could exist in a graphene matrix as for a cobalt-carbon or copper-carbon case.[25] Banhart *et al.*[26] (1998) and Abe *et al.*[27] (2001) observed, at high temperature, a progressive shrinkage of the metallic (gold, cobalt, or copper) nanoparticle and the formation of hollow carbon spheres. In particular, Banhart *et al.*[26] (1998) proposed a mechanism in which the presence of defects such as carbon heptagons, which were assumed to exist in spherical shells, or octagons would be responsible for an enhanced diffusion of the atomic species. Indeed, TEM observation of the carbon spheres revealed the presence of defects such as discontinuities of the graphene layers, and this could explain the penetration of silver species through the graphene layers. Moreover, an external coherent graphene layer could also apply a high pressure onto the encapsulated silver species that initiated the diffusion of the silver outside of the nanosphere.[24] In addition, carbon encapsulated silver nanoparticles [white circles in Fig. 4(b)] also existed on the nanospheres, which might have resulted from displaced silver species (maybe they did not nucleate in carbon shell) or nonencapsulated silver species (maybe they solely existed in the gas flow).

In summary, three kinds of nanostructure, carbon encapsulated silver nanoparticles, multiwall carbon nanotubes, and hollow carbon nanospheres, were fabricated through a silver-carbon ambient spark. The cooling process near the spark channel was critical in determining the nanostructure growth:[15] for $-2{,}900$ K s^{-1}, steep temperature gradients could be obtained, leading to a high nucleation rate, which allowed a tubelike graphitization of carbon on silver nanoparticles; while spheroidization (nanoparticles are expected to have smooth spherical shapes) of carbon and silver precursors and their crystallization were achieved for $<-1{,}400$ K s^{-1} cases due to the longer high-temperature-exposure effects, resulting in formation of hollow and encapsulated spherical nanostructures.

[1] N. Sano and M. Uehara, Chem. Eng. Process. **45**, 555 (2006).
[2] K. H. Ang, I. Alexandrou, N. D. Mathur, G. A. Amaratunga, and S. Haq, Nanotechnology **15**, 520 (2004).
[3] I. Levchenko, K. Ostrikov, and D. Mariotti, Carbon **47**, 344 (2009).
[4] C. P. Collier, P. J. Sayally, J. J. Shiang, S. E. Henrichs, and J. R. Heath, Science **277**, 1978 (1997).
[5] W. P. McConnell, J. P. Nova, L. C. Brousseau, R. R. Fuierer, R. C. Tenent, and D. L. Feldheim, J. Phys. Chem. B **104**, 8925 (2000).
[6] N. R. Jana, T. K. Sau, and T. Pal, J. Phys. Chem. B **103**, 115 (1999).
[7] S. Y. Wu, Y. S. Ding, X. M. Zhang, H. O. Tang, L. Chen, and B. X. Li, J. Solid State Chem. **181**, 2171 (2008).
[8] W.-J. Liu, Z.-C. Zhang, W.-D. He, C. Zheng, X.-W. Ge, J. Li, H.-R. Liu, and H. Jiang, J. Solid State Chem. **179**, 1253 (2006).
[9] D. Cheng, X. Zhou, H. Xia, and H. S. O. Chan, Chem. Mater. **17**, 3578 (2005).
[10] T. Oku, T. Kusunose, T. Hirata, R. Hatakeyama, N. Sato, K. Niihara, and K. Suganuma, Diamond Relat. Mater. **9**, 911 (2000).
[11] X. M. Sun and Y. D. Li, Langmuir **21**, 6019 (2005).
[12] A. A. Antipov, G. B. Sukhorukov, Y. A. Fedutik, J. Hartmann, M. Giersig, and H. Möhwald, Langmuir **18**, 6687 (2002).
[13] V. G. Pol, H. Grisaru, and A. Gedanken, Langmuir **21**, 3635 (2005).
[14] J. H. Byeon, J. H. Park, and J. Hwang, J. Aerosol Sci. **39**, 888 (2008).
[15] K. Ostrikov and A. B. Murphy, J. Phys. D **40**, 2223 (2007).
[16] M. Keidar, I. Levchenko, T. Arbel, M. Alexander, A. M. Waas, and K. Ostrikov, Appl. Phys. Lett. **92**, 043129 (2008).
[17] J. H. Byeon, J. H. Park, K. Y. Yoon, and J. Hwang, Nanoscale **1**, 339 (2009).
[18] J. H. Byeon and J.-W. Kim, ACS Appl. Mater. Interfaces, doi:10.1021/am100015a.
[19] Z. Kang, E. Wang, S. Lian, L. Gao, M. Jiang, C. Hu, and T. Oda, Nanotechnology **15**, 490 (2004).
[20] R. Ono, M. Nifuku, S. Fujiwara, S. Horiguchi, and T. Oda, J. Appl. Phys. **97**, 123307 (2005).
[21] T. Y. Kosolapova, *Handbook of High Temperature Compounds: Properties, Production, Applications* (Hemisphere, New York, 1990).
[22] L. S. Wang, D. B. Buchholz, Y. Li, J. Li, C. Y. Lee, H. T. Chiu, and R. P. H. Chang, Appl. Phys. A: Mater. Sci. Process. **87**, 1 (2007).
[23] G. E. Gadd, M. Collela, M. Blackford, A. Dixon, P. J. Evans, D. McCulloch, S. Bulcock, and D. Cockayne, Carbon **39**, 1769 (2001).
[24] E. Thune, Th. Cabioc'h, M. Jaouen, and F. Bodart, Phys. Rev. B **68**, 115434 (2003).
[25] D. Babonneau, T. Cabioc'h, A. Naudon, J. C. Girard, and M. F. Denanot, Surf. Sci. **409**, 358 (1998).
[26] F. Banhart, Ph. Redlich, and P. M. Ajayan, Chem. Phys. Lett. **292**, 554 (1998).
[27] H. Abe, S. Yamamoto, A. Miyashita, and K. E. Sickafus, J. Appl. Phys. **90**, 3353 (2001).